A Feasiblity Study of Elastography Based Confocal Microwave Imaging Technique for Breast Cancer Detection

Jinzu Ji[a,*], Kin-Fai Tong[b], Allan Al-Armaghany[b], Terence S. Leung[c]

[a] *School of Aeronautic Science and Engineering, Beihang University, Beijing, 100191, China*
[b] *Department of Electronic and Electrical Engineering, University College London, London, WC1E6BT, UK*
[c] *Department of Medical Physics and Biomedical Engineering, University College London, London, WC1E6BT, UK*

Abstract

Breast cancer is a common cancer type in women and its death rate is second highest among different kind of cancers. Early detection is an efficient way for curing and recovery. Confocal microwave imaging (CMI) using electromagnetic method for detection of breast cancer can avoid ionization caused by mammography. CMI uses the contrast of electrical properties between tumor and normal breast tissue to identify the existence and location of the tumor. However, new research result shows that gland and tumor have similar dielectric constant and electrical conductivity, so it is hard to distinguish gland and tumor. This paper proposes a new method based on elastography for the tumor identification. The high Young's modulus contrast of the two tissues resulting in different level of deformation by compression will provide sufficient features to discriminate whether the reflected signal is belonged to gland or tumor. Finite-difference time-domain (FDTD) method was used in simulation. Some examples were presented to validate the identification.

Keywords: microwave imaging, breat cancer, detection, Young's modulus, compression, identification

*Corresponding author
Email addresses: jijinzu@buaa.edu.cn (Jinzu Ji), k.tong@ucl.ac.uk (Kin-Fai Tong), t.leung@ucl.ac.uk (Terence S. Leung)

1. Introduction

Every year, there are millions of women being diagnosed as breast cancer patient and suffering from it. Regular examination is very important for early-stage cancer detection. Nowadays, the most widely used method is mammography, using X-ray to detect the existence and location of tumor. But X-ray will raise the probability of cancer cue to the ionizing. In addition, the mammography method has high positive-false and negative-false in detection.

Using microwave for detection of breast is recently reported [1, 2, 3, 4, 5, 6, 7, 8, 9, 10, 11]. The method relies on two basic properties of breast tissues: 1) the high contrast in electrical properties between tumor and normal breast tissue. The tumor's dielectric constant is about five times higher than normal breast tissue and the conductivity is about ten times higher. Such significant difference can bring enough information for detection. 2) The energy absorption of normal breast tissue is relatively small, so that the microwave energy can penetrate it and sufficient backscatter energy can return back to the antennas.

Many types of microwave imaging method have been raised in the past decades, such as confocal microwave imaging (CMI) [1, 2, 3, 4, 5, 6, 7, 8], spatial time beam forming method (STBF) [9] , time reversal method (TR) [10, 11] and so on. CMI is the simplest one for its antenna array arranging and data process. Elahi et al used graphical process unit (GPU) to accelerate CMI algorithms for breast cancer detection [12]. Medina et al compared confocal and holography algorithms in mMicrowave imaging for breast cancer detection by experiments [13]. This paper's algorithm is based on the CMI and makes use of the target's deformation after compression of breast.

Recent study shows that gland and tumor have quite similar electrical properties both in dielectric constant and conductivity [14]. It is because of the two types of tissues have similar water content in them and the water content mainly determines the electrical property.

In elastography, different mechanical properties of various breast tissues are studied [15]. Results show that the Young's modulus of gland and tumor are

quite different, the latter is almost 18 times higher than the former. Meanwhile, the Young' modulus of a normal breast tissue is quite similar to that of a gland. Based on these facts, we predict that after breast compression the deformation of tumor and gland might be quite different. CMI method can be used to form the shape of the target, and different level of deformation of the target shape before and after compression of the breast can illustrate where it is tumor or gland.

During diagnosis, there are two patient positions in CMI, namely supine and prone. In supine position, the patients lie on their back and the antennas are put on the breast skin. In prone position, the patients lie on their front with the breast extending into a hole on the examination table. The breast was emerged in liquid which has similar electrical properties with the breast to reduce the reflection from the skin. Prone position is assumed for CMI simulation in this paper. The antenna takes turns of transmitting and receiving signals in seventeen different positions around the breast. The transmitting signal is a differentiated Gaussian pulse shown in Equation (1)

$$s(t) = 2\left(\frac{t-t_0}{\tau}\right)e^{\left(\frac{t-t_0}{\tau}\right)^2} \tag{1}$$

where $\tau = .625$nm, $t_0 = 4\tau$. Choose τ carefully, so that differentiated Gaussian pulse has a peak at 5 GHz.

Two-dimensional Finite-difference time-domain (FDTD) algorithm was used for simulation. The breast model was an infinitely long 60-mm-diameter-cylinder with 2-mm-thickness-skin. The simulation area is a 100×100mm square terminated by Mur second-order absorbing boundary condition (ABC). The antenna has a distance of 40 mm from the center of the model, so it is about 8 mm away from the skin. The polarization in simulation is transverse magnetic (TM), that is, the electric field is along the infinite axis.

Every detection simulation consists of two sub simulations. One is for uncompressed breast, that is, natural state, and the other is for compressed breast. After compression, the tumor or the gland will deform differently according to

their stiffness governed by the Young's modulus.

The remains of the paper are arranged as follows. Section 2 shows the breast model setting and the antenna array arrangement. Section 3 discusses the CMI algorithm to image the target. Section 4 presents the simulation result and analysis of the difference of the compression. Section 5 is summaries and conclusions.

2. Model setting

The Finite-Difference Time-Domain (FDTD) grid is set to be 0.4 mm, therefore the total grid is 250×250 within the area of 100×100mm. The calculation area and the antenna array position are shown in Figure 1. The figure shows the uncompressed with tumor in it. Because the tumor's stiffness is eighteen times higher than the normal breast tissue, the tumor seldom deformed.

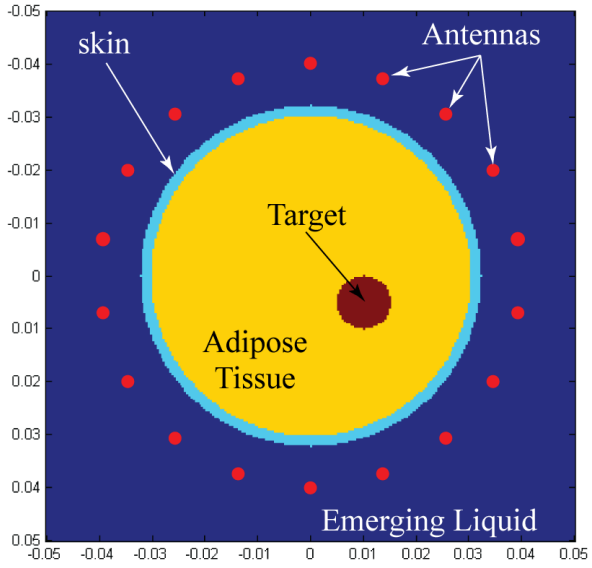

Figure 1: The simulation geometry of an uncompressed breast. The red dots mark the locations of the antenna elements.

The nominal electrical properties of various tissues in breast are tabulated in Table 1.

Table 1: Electrical properties of the tissues in the simulation model [5]

Tissues	Dielectric constant	Conductivity ($\mathrm{S\,m^{-1}}$)
Emerging liquid	9	0
Skin	36	4
Normal breast tissue	9	0.4
Tumor and gland	50	4

The Young's moduli of adipose tissue, gland and tumor are 0.04 kPa,0.05 kPa and 0.9 kPa, respectively[15].

For demonstrating the idea, the compression ratio is first set at 0.7 in vertical direction and remains unchanged in the other direction. We simulate the deformation of the breast and target based on the Saint-Venant principle in material science: When a force is applied to an object, the local deformations caused can be considered as on the basis of the entire object, rather than at the point of application. In this case, the stress σ is unique near the target area, therefore, we have

$$\sigma = E_{\mathrm{a}}\varepsilon_{\mathrm{a}} = E_{\mathrm{g}}\varepsilon_{\mathrm{g}} = E_{\mathrm{t}}\varepsilon_{\mathrm{t}} \tag{2}$$

where E_{a}, E_{g} and E_{t} are the Young's modules, and ε_{a}, ε_{g} and ε_{t} are strain of the adipose tissues, gland and tumor respectively. When the deformation of the adipose tissue in the breast is 0.7, the strain is 0.3 and the strain of gland and tumor inside are 0.24 and 0.0133, respectively. The gland and tumor's deformations are 0.76 and 0.9867, respectively. The simulated deformation of tumor and gland are shown in Figure 2.

In Figure 2, we can see that there is significant difference between the deformation of the tumor and the gland due to the stiffness contrast. Therefore, if we can image the compressed breast, the image of the deformed target can provide useful information on whether the target is tumor or gland.

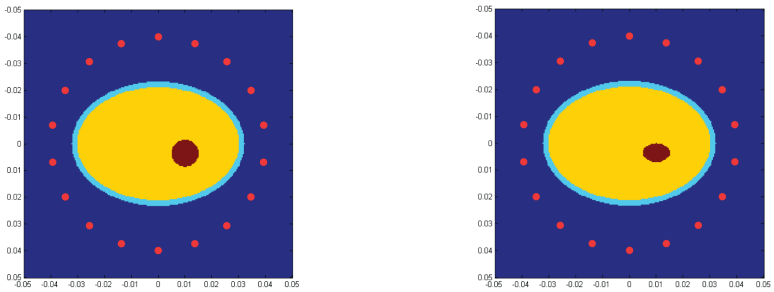

(a) (b)

Figure 2: Deformation of (a) tumor, and (b) gland after compression

3. Algorithm of confocal microwave imaging

The reflections from a normal breast are first simulated, so the target's reflection can be isolated by subtracting the normal breast reflection from the total reflection of the breast with a target. The two simulations used the same antenna array and skin/breast model.

The antenna elements radiate separately and when one antenna is radiating, the rest seventeen will be receiving. Every received signal from different radiating element was accumulated to generate a maximum at the time corresponding to the target's position. For example, Antenna 1, Antenna 2, the received signals before and after accumulation are shown in Figure 3.

As we can see from Figure 3b that after accumulation, there are peaks on each signal replacing the zeros at the same time interation points in original signal. The position of maximum peaks is due to the strong scattering distance.

Every pixel within the breast is traversed to calculate scattering intensity of that point and was shifted due to the round-trip of the signal from the antenna to the pixel. The signal propagation attenuation was scaled by factor of $1/r^2$, where r is the separations from each antenna to the pixel. The scattering signals at corresponding time from each antenna were added up coherently. On the strong scattering pixels, the summation is bigger and on other pixels it

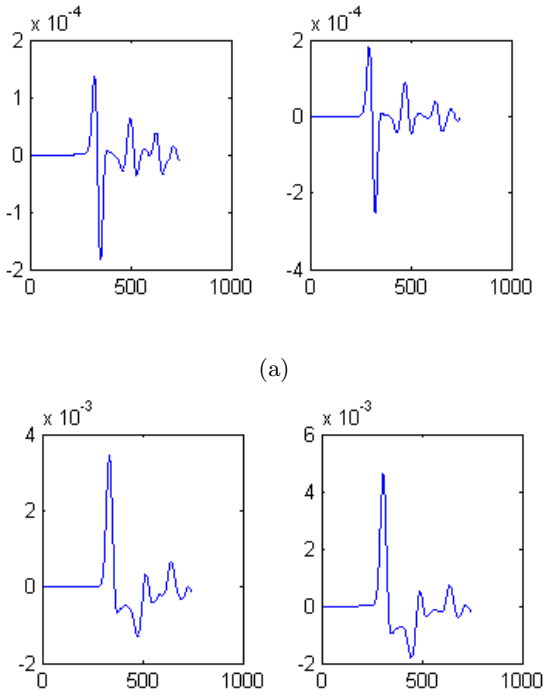

Figure 3: Received signals (a) before accumulation, and (b) after accumulation.

is smaller. Therefore, the CMI imaging will illustrate the distribution of the scattering.

4. Result and analysis

4.1. result of tumor and gland

The CMI imaging using a circular antenna array of an uncompressed breast with a target of 10 mm diameter inside is shown in Figure 4.

As shown in Figure 4, the imaged result illustrates the correct shape and position of the target when compared to Figure 1. However, because of the similarity of the dielectric properties of the gland and tumor, at this stage it is not possible to identify which kind the target it is.

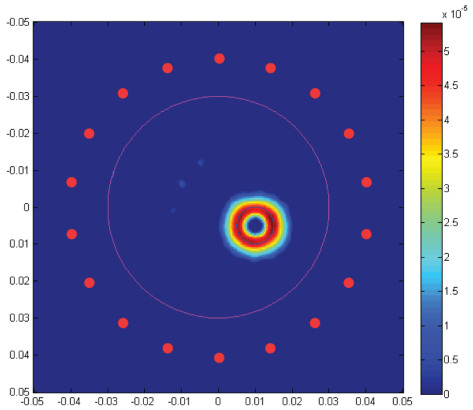

Figure 4: Reflection image of an uncompressed breast with a suspected target after accumulation.

We propose to utilize the significant difference of Young's modulus between tumor and gland to identify the two tissues. The breast is compressed to 0.7 times of the original size in one direction and remains the same in another direction as mentioned in Section 2. The tumor and gland have different stiffness, so we get different deformation of the target even though the breast has the same deformation.

The deformations of the tumor and gland are shown in Figure 2. We can see from the figure that the tumor and the gland have quite different deformation. The deformation is estimated using Young's modulus via Saint Vennant principle. The two deformed models are imaged by the same CMI method and the imaging results are shown in Figure 5.

345.0pt

In Figure 5, it can be observed that the profiles of the images are similar to that of the targets' own shapes. However, the profiles of the tumor and the gland images are quite different. The imaged shape of a tumor is close to a circle while the gland's imaging shape is oval. And this is the result of the different deformation. Therefore by comparison of the images of the target inside a compressed and uncompressed breast, we can identify if the target is

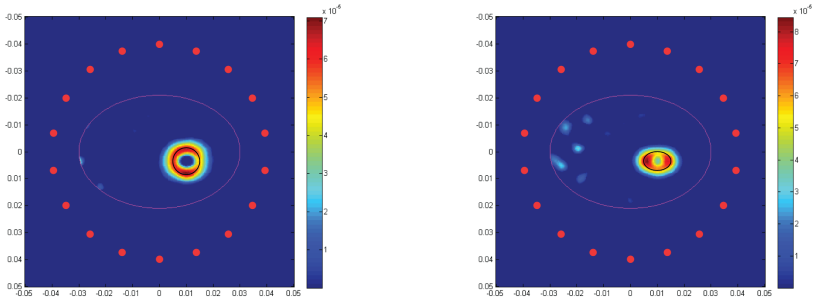

(a) (b)

Figure 5: CMI imaging results of (a) tumor, and (b) gland using the circular array.

tumor or gland.

4.2. Conformal antenna array arrangement

To further confirm the reliability of the results and compare the influence from different antenna arrangements, we used a conformal antenna array arrangement in which the distances from the antenna to the skin remain the same before and after the compression of the breast. Same number of antenna is arranged in the array at the same position and the same breast model described in Section 2 is used. The conformal antenna arrangement in vertical compression is shown in Figure 6. In practical application, the array requires precisely confirmation of antennas' position and is more complicated, however such conformal design can be realized by using soft and flexible dielectric material.

The CMI images of the two different targets are shown in Figure 7. By comparing Figure 5 and Figure 7, we can observed: 1) distinguishable image profiles can be obtained from the conformal array as well, 2) the tumor image look similar in both antenna arrangement, 3) noticeable difference can be observed between the two gland images, as higher contrast is achieved in the gland image when using conformal array.

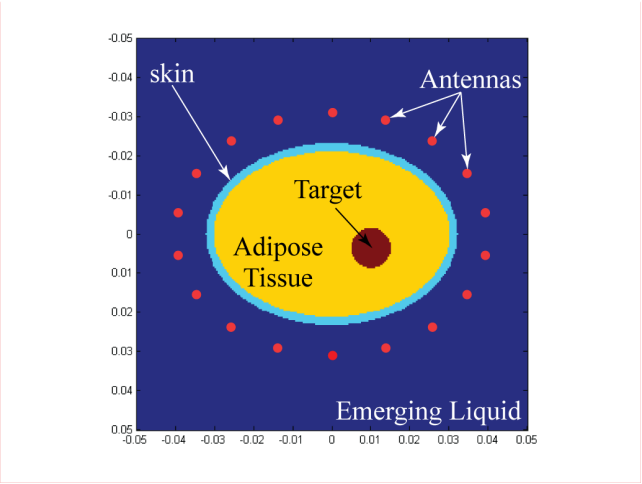

Figure 6: The simulation geometry of an compressed breast. The red dots mark the locations of the antenna elements.

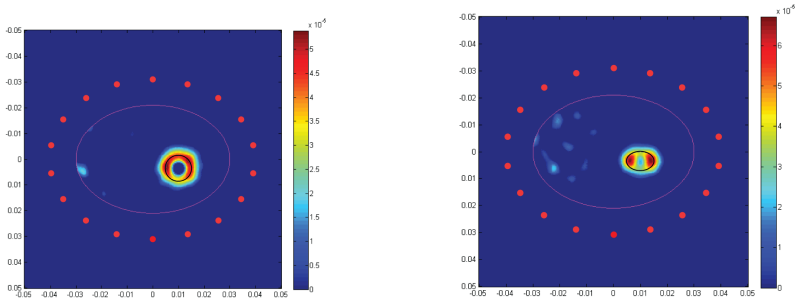

(a) (b)

Figure 7: CMI images of (a) tumor, and (b) gland using the conformal antenna array.

4.3. Investigation of the stiffness influence

Various targets with different stiffness have been studied to show the changes caused by the stiffness of the target to the image. The deformation ratios are due to the different Young's moduli. Table 2 shows the deformation ratio corresponding to the Young's modulus.

From Table 2 we see that the tougher the target, the less deformation. We conducted the simulation and imaging of these different deformations of targets

Table 2: Young's modulus of different tissues in the model

Young's modulus relative to normal breast tissue	Strain of target	Deformation ratio
20 (nominal tumor)	0.015	0.985
3	0.1	0.9
1.5	0.2	0.8
1.03 (nominal gland)	0.29	0.71

as shown in Figure 8.

From Figure 8, we see that the images can show the boundary of the targets in different shapes. The comparison of the target images with the uncompressed result can show the stiffness. Therefore, the scatterer is tumor or the gland can be identified.

5. Conclusion

The imaging results of the compressed breast are quite different according to the different deformation of scatterers due to stiffness. By the method presented in this paper, we can identify if the scatterer is tumor or gland, and provide more reliable results to the surgeons.

References

[1] S. C. Hagness, A. Taflove, J. E. Bridges, Three-dimensional fdtd analysis of a pulsed microwave confocal system for breast cancer detection: design of an antenna-array element, IEEE Transactions on Antennas and Propagation 47 (5) (1999) 783–791. doi:10.1109/8.774131.

[2] L. Xu, S. C. Hagness, A confocal microwave imaging algorithm for breast cancer detection, IEEE Microwave and Wireless Components Letters 11 (3) (2001) 130–132. doi:10.1109/7260.915627.

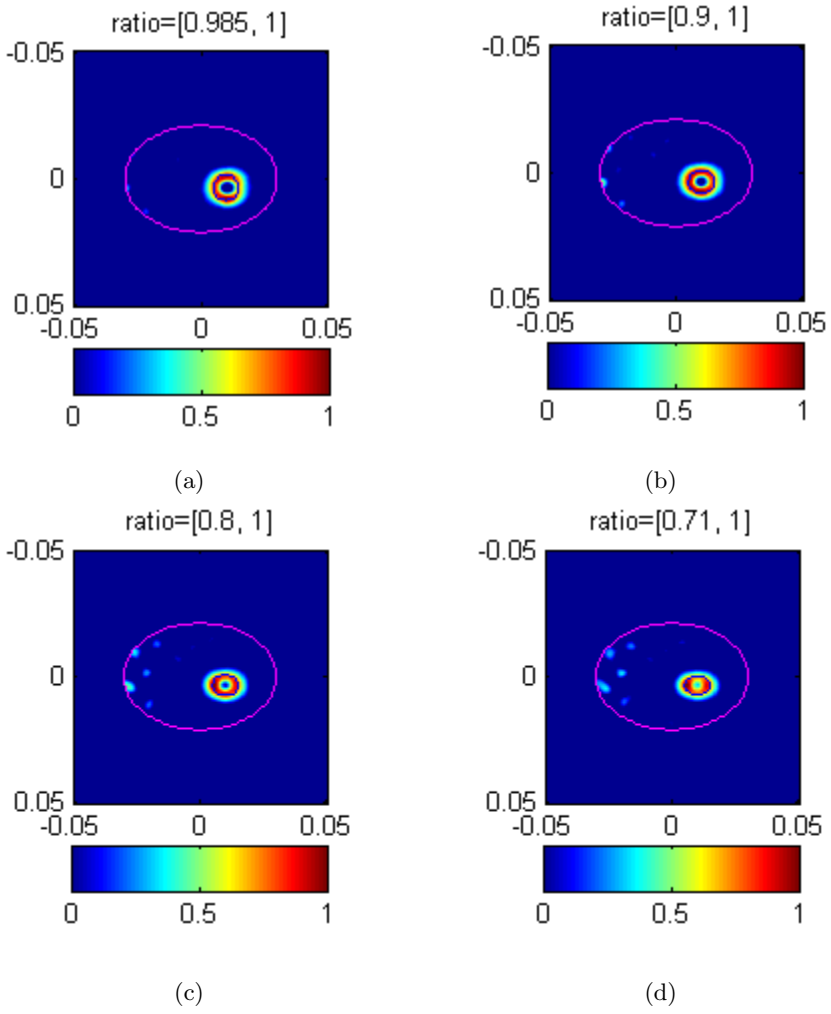

Figure 8: CMI images of targets of different level of deformation under the same deformation of breast. (The first and second number in the bracket is the deformation ratios in the vertical and horizontal direction, respectively.)

[3] H. B. Lim, N. T. T. Nhung, E. P. Li, N. D. Thang, Confocal microwave imaging for breast cancer detection: Delay-multiply-and-sum image reconstruction algorithm, IEEE Transactions on Biomedical Engineering 55 (6) (2008) 1697–1704. doi:10.1109/TBME.2008.919716.

[4] S. C. Hagness, A. Taflove, J. E. Bridges, Correction to "two-dimensional

fdtd analysis of a pulsed microwave confocal system for breast cancer detection: Fixed-focus and antenna-array sensors", IEEE Transactions on Biomedical Engineering 46 (3) (1999) 364–364. doi:10.1109/TBME.1999.748990.

[5] E. C. Fear, M. A. Stuchly, Microwave detection of breast cancer, IEEE Transactions on Microwave Theory and Techniques 48 (11) (2000) 1854–1863. doi:10.1109/22.883862.

[6] M. Klemm, I. J. Craddock, J. A. Leendertz, A. Preece, R. Benjamin, Radar-based breast cancer detection using a hemispherical antenna array—experimental results, IEEE Transactions on Antennas and Propagation 57 (6) (2009) 1692–1704. doi:10.1109/TAP.2009.2019856.

[7] E. C. Fear, X. Li, S. C. Hagness, M. A. Stuchly, Confocal microwave imaging for breast cancer detection: localization of tumors in three dimensions, IEEE Transactions on Biomedical Engineering 49 (8) (2002) 812–822. doi:10.1109/TBME.2002.800759.

[8] E. C. Fear, J. Sill, M. A. Stuchly, Experimental feasibility study of confocal microwave imaging for breast tumor detection, IEEE Transactions on Microwave Theory and Techniques 51 (3) (2003) 887–892. doi:10.1109/TMTT.2003.808630.

[9] L. Xu, S. K. Davis, S. C. Hagness, D. W. v. d. Weide, B. D. V. Veen, Microwave imaging via space-time beamforming: experimental investigation of tumor detection in multilayer breast phantoms, IEEE Transactions on Microwave Theory and Techniques 52 (8) (2004) 1856–1865. doi:10.1109/TMTT.2004.832686.

[10] P. Kosmas, C. M. Rappaport, Fdtd-based time reversal for microwave breast cancer detection-localization in three dimensions, IEEE Transactions on Microwave Theory and Techniques 54 (4) (2006) 1921–1927. doi:10.1109/TMTT.2006.871994.

[11] P. Kosmas, C. M. Rappaport, A matched-filter fdtd-based time reversal approach for microwave breast cancer detection, IEEE Transactions on Antennas and Propagation 54 (4) (2006) 1257–1264. doi:10.1109/TAP.2006.872670.

[12] M. A. Elahi, A. Shahzad, M. Glavin, E. Jones, M. O. Halloran, Gpu accelerated confocal microwave imaging algorithms for breast cancer detection, in: 2015 9th European Conference on Antennas and Propagation (EuCAP), pp. 1–2.

[13] Y. Medina, M. Augusto, A. V. Paz, Microwave imaging for breast cancer detection: Experimental comparison of confocal and holography algorithms, in: 2016 IEEE ANDESCON, pp. 1–4. doi:10.1109/ANDESCON.2016.7836226.

[14] M. Lazebnik, D. Popovic, L. McCartney, C. B. Watkins, M. J. Lindstrom, J. Harter, S. Sewall, T. Ogilvie, A. Magliocco, T. M. Breslin, W. Temple, D. Mew, J. H. Booske, M. Okoniewski, S. C. Hagness, A large-scale study of the ultrawideband microwave dielectric properties of normal, benign and malignant breast tissues obtained from cancer surgeries, Physics in Medicine and Biology 52 (20) (2007) 6093–6115. doi:10.1088/0031-9155/52/20/002.
URL <GotoISI>://WOS:000250443400002

[15] M. M. Dastjerdi, A. Mahloojifar, Towards realistic modeling of breast elasticity modulus alterations in medical simulation, in: 2008 IEEE International Symposium on Knowledge Acquisition and Modeling Workshop, pp. 1148–1151. doi:10.1109/KAMW.2008.4810699.